AGU PUBLICATIONS

Raquel Somavilla

Supporting Information for

The warmer the ocean surface, the shallower the mixed layer. How much of this is true?

R. Somavilla[1], C. González-Pola[1], J. Fernandez[2]

[1]Instituto Español de Oceanografía, [2]Universidad de Oviedo

Contents of this file

Introduction

This Supporting Information provides detailed information about the subsections 'Data sources' (1.1) and 'Winter MLD trends and its forcing' (1.2) resumed in the main body of the manuscript in subsections 2.1 and 2.4, respectively. Auxiliary results providing climatological seasonal cycles from ORAS4 and Argo floats, and seasonal cycles and long term variability from MLD determination methods MLD_{HT} and $MLD_{\Delta\sigma}$ are also included.

1. Material and Methods.

1.1. Data sources.

The investigation of long term changes in MLD and stratification concurrent with surface warming trends are based on standard hydrographic observations (salinity and temperature profiles) at oceanographic sections regularly visited in the mid-latitudes of the eastern North Atlantic (ml-ENA) and in the subtropical gyres of the North Atlantic (sg-NAtl) and North Pacific (sg-NPac), Argo floats and reanalysis products (ECMWF Ocean Reanalysis System 4, ORAS4) (Balmaseda et al. 2013b) in the regions of interest.

In the ml-ENA, northwards of Santander in the Bay of Biscay, an oceanographic section (Santander Atlantic Time-Series, SATS) is monthly visited since 1991 as part of the Radiales program of the Spanish Institute of Oceanography (www.seriestemporales-ieo.es). Due to the proximity of the shelf break to the coast near Santander, the northernmost station of the section (43° 48'N, 3° 47' W, see Fig. 1) is oceanic, located at a depth of 2580 m. The station is representative of air-sea interaction conditions and mixed layer depth variability at mid-latitudes of the ENA (Somavilla et al. 2009, 2011, 2016), and it is a valuable tool for water mass variability analysis (González-Pola et al. 2005). The sampling at this station began in August 1994. Since then, a SBE25 or SBE911+ CTD models have been used, and water samples are taken for salinity determinations for calibration purposes. Data set are archived at the Spanish Institute of Oceanography (http://indamar.ieo.es) where they can be requested.

In the sg-NAtl, the Bermuda Atlantic Time-series Study (BATS) was established to help scientists fully understand how the ocean responds to global climate change. The program began in 1988, and since then monthly hydrographic and biogeochemical measurements are collected at the BATS site (32.2° N, 64.5° W). Starting in January 1990, biweekly measurements have been made during the winter/spring bloom period (January to April). The BATS data are available from the Bermuda Institute of Ocean Sciences/Bermuda Atlantic Time-series Study web page (http://bats.bios.edu/). Specific details and information about the data can be found on the web page. BATS data have been used by researchers at BIOS--and around the globe--to explore active oceanographic questions and integrate new methodologies into their research.

In the sg-NPac, the Hawaii Ocean Time-series (HOT) was established at a station north of Oahu, Hawaii in October 1988. Since then, the program have been making repeated observations of the hydrography, chemistry and biology of the water column to provide a comprehensive description of the ocean at a site representative of the North Pacific subtropical gyre. Cruises are made approximately once per month to the deep-water Station ALOHA (A Long-Term Oligotrophic Habitat Assessment; 22.8° N, 158°W) located 100 km north of Oahu, Hawaii. Measurements of the thermohaline structure, water column chemistry, currents, optical properties, primary production, plankton community structure, and rates of particle export are made on each cruise. HOT data are available from the Hawaii Ocean Time-series web page (http://hahana.soest.hawaii.edu/hot/). Specific details and information for the data can be found on the web page under HOTS Information/Methods.

Systematically along the work, temperature and salinity time-series from oceanographic sections are presented together with those constructed from Argo floats and ORAS4 ocean reanalysis data. Data from Argo floats and ORAS4 in Figures 4 and 5 in the main text have been

extracted in 4°x4° boxes centered at the position of the oceanographic time-series. In this way, we prove the representation of the changes detected at oceanographic sections of larger oceanic areas, and, on the other hand, it serves as an important validation both for Argo floats and gridded data sets affected by e.g. the changes in observation coverage around 2005 (Roemmich et al., 2015) and contamination from model error in ocean reanalysis data (Balmaseda et al., 2013).

The Argo float data have been downloaded from Coriolis Data Center (ftp://ftp.ifremer.fr/ifremer/argo/). Only good data according to Argo standards have been retained, and floats included in the grey list have been removed from the data set. The Argo float temperatures are accurate to ±0.005°C and uncorrected salinities to ±0.01, although delayed-mode correction can reduce further salinity errors. The ORAS4 reanalysis provides monthly temperature, salinity, current and sea level data at 42 pressure levels from 5 to 5000 m with higher vertical spacing towards the bottom and a spatial resolution of 1°x1°.

The weekly optimum interpolated NOAA_OI_SST_V2 data set (OISST), which is mainly supported by satellite data but also integrating in situ data plus simulated SST is used in this work to evaluate sea surface warming.

Surface fluxes data (net heat fluxes, precipitation rate and wind stress zonal and meridional components) from NCEP/NCAR Reanalysis data set (Kalnay et al. 1996) have been used to estimate the effects of buoyancy fluxes and Ekman pumping on MLD winter deepening. The NCEP/NCAR Reanalysis data set developed between the National Centers for Environmental Prediction (NCEP) and the National Center for Atmospheric Research (NCAR) has become the most popular Reanalysis data set used. Data are available since 1948 onwards providing a broad set of parameters and fluxes as 6 hourly, daily and monthly values (http://www.esrl.noaa.gov/psd/data/gridded/data.ncep.reanalysis.html).

1.2. Winter MLD trends and its forcing.

1.2.1. Changes on winter MLD due to changes in the buoyancy forcing and stratification.

During autumn-winter, buoyancy losses from cooling and/or evaporation make the ocean surface to become colder and saltier (densification of the ocean surface) and induce convective mixing and overturning that cause the surface properties to mix with deeper water. These processes control the erosion of the seasonal pycnocline during autumn and further deepening of the MLD during the winter. Thus, the integration in time of the buoyancy forcing during the autumn-winter time enables to estimate the vertical extension of the winter MLD (h) -and so comparable to the winter MLD averages- as:

$$h = \left[\frac{2 \int_{t_0}^{t_f} B_0 dt}{N^2} \right]^{1/2}$$

where Bo is the buoyancy forcing and N^2, the Brunt-Vaisala frequency. Thus, for each year, we estimate the vertical extent of the winter mixed layer as a result of the integration in time of the buoyancy forcing (Bo) during the complete autumn-winter period. The autumn-winter period is not fixed but defined as the time of the year (from t_o to t_f) when climatologically Bo is negative

(coinciding with the time period when climatologically SST is decreasing), since this is the time of year when convective mixing and progressive deepening of the mixed layer can occur. During this time of the year the seasonal pycnocline is progressively eroded. Thus, we use the mean value of N^2 just below the summer mixed layer and until the base of the climatological maximum MLD at the end of the winter found in ocean observations during the autumn-winter each year as representative of the stratification that will exert opposition to mixed layer deepening by Bo. Dividing the integration in time of Bo by the corresponding N^2 each year, the MLD reach at the end of the winter (h) is the square root of this value. Using this expression, the expected changes in winter MLD in each of the study areas according to changes in (1) winter buoyancy fluxes estimated from surface heat fluxes from NCEP/NCAR reanalysis data and (2) stratification observed in oceanographic time-series are calculated.

Buoyancy fluxes are estimated from surface heat fluxes from NCEP/NCAR reanalysis as in Somavilla et al. (2009) following the scheme presented in the work of Josey (2003). The combined impact of the net heat flux Qo and the net evaporation (E-P) (difference between evaporation and precipitation) on the buoyancy of water in the sea surface layer is expressed in terms of the density flux F_ρ, which may be expressed as the addition of thermal (as a result of heat fluxes, Qo) and haline (as a result of fresh water fluxes, E-P) contributions, hence,

$$F_\rho = F_t + F_s,$$

where

$$F_t = -\alpha \frac{Q_0}{C_p} \quad , \quad F_s = \rho \cdot \beta \cdot S \frac{E - P}{(1 - S/1000)},$$

where ρ is the density of water at sea surface; C_p, the specific heat capacity of water; α and β, the thermal and haline contraction coefficients, respectively; and S, the sea surface salinity (SSS).

Qo, the net heat flux through the ocean surface is given by the sum of four components: Q_E is the latent heat flux; Q_H, the sensible heat flux; Q_{lw}, the longwave flux; and Q_{sw} the shortwave flux. All these surface heat fluxes and the precipitation rate (P) can be obtained from NCEP/NCAR reanalysis data set. The evaporation rate (E) is calculated as $Q_E/L_e \cdot \rho_o$ where L_e is the latent heat of vaporization, and ρ_o is the reference density of seawater (1027.0 $kg \cdot m^{-3}$). The sign convention is as follows: the net heat flux is negative, Qo<0, when indicates heat loss from the ocean to the

atmosphere. Negative net heat flux (heat loss), and positive net evaporation, E-P>0, result in positive values for F_t and F_s respectively and in an increase in the density of the near surface layer.

There is a simple relationship between the density flux and the buoyancy flux B given by the following equation Sil94:

$$B = g \cdot F_\rho$$

where g is the acceleration due to gravity. With the sign convention followed, an increase in the density of the ocean surface corresponds to a buoyancy loss.

1.2.2. Changes on winter MLD due to changes wind-driven divergence/convergence.

The horizontal variability of the wind stress (τ) over the sea surface leads to variability of the horizontal transports (Ekman transports). Because mass must be conserved, the spatial variability of the transports lead to vertical non-turbulent velocities (w_{EK}) that pump the upper ocean surface layer solely as a result of divergences/convergences driven by wind stress curl (see schematic of the process in Fig. 8 in the main text). The w_{EK} is related to the wind stress curl through the expression:

$$w_{EK} = curl\left(\frac{\tau}{\rho f}\right) \quad w_{EK} = -\frac{1}{\rho} \cdot \left[\frac{\delta \tau_y}{\delta x \cdot f} - \cdot \frac{\delta \tau_x}{\delta y \cdot f}\right]$$

Following this expression and using the zonal (τ_x) and meridional (τ_y) components of the wind stress obtained from NCEP/NCAR Reanalysis data set, we have calculated for each grid point in the maps shown in Fig. 9a and c in the North Pacific and North Atlantic their corresponding w_{EK} time-series. The resulting daily Δh_{EK} from these time-series (daily Δh_{EK} = daily w_{EK} ($m \cdot s^{-1} \cdot 3600 \cdot 24$) are shown here in Fig. S1 for the locations of the oceanographic time-series in the sg-NPac, sg-NAtl and ml-ENA. The original time-series (Fig. S1a, b anc c) may give the impression that w_{EK} simply oscillates between positive and negative values, but the accumulated time-series show clearly that at the position of the oceanographic time-series in the sg-NPac the water column is pumped upwards and in the sg-NAtl downwards (Accumulated Δh_{EK} after 25 years is almost

approximately +600 m and -600 m, respectively (Fig. S1d, e)). In the ml-ENA is almost zero until 2005 changing after that (Fig. S1f).

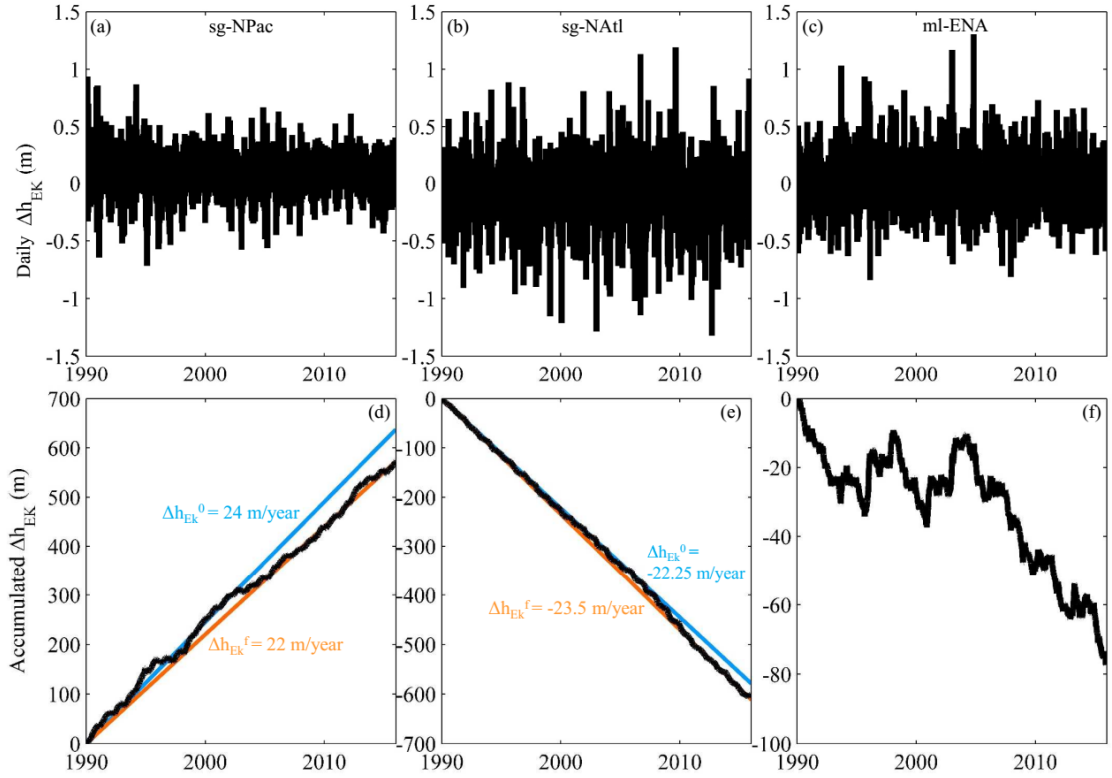

Figure S1. (a), (b), and (c) Daily Δh_{EK} generated by w_{EK} at the position of oceanographic time-series in the sg-NPac, sg-NAtl, and ml-ENA. (d), (e), and (f) Accumulated Δh_{EK} over time. Constant h_{EK} per year able to generate the accumulated Δh_{EK} in the sg-NPac and sg-NAtl are shown by the blue and orange lines. The blue ones indicate the constant Δh_{EK} per year observed at the beginning of the time-series (Δh_{EK}^{0}) and the orange ones at the end (Δh_{EK}^{f}).

For each time series corresponding to a particular grid point (Fig. S1a, b, and c), the winter average w_{EK} has been calculated, and the integrated vertical displacement (Δh_{EK}) that it generates throughout the winter calculated (e.g. a w_{EK} of $3.5 \cdot 10^{-6}$ $m \cdot s^{-1}$generates a winter Δh_{EK} of 30 m). The average winter Δh_{EK} as a result of wind-driven divergence/convergence at the different locations in the North Atlantic and North Pacific are shown in Fig. 9a and c. Additionally, for each of these w_{EK} time series corresponding to a particular grid point, the changes in the

winter w_{EK} over time have been calculated as linear regression of the changes in the winter w_{EK} over time (Δh_{EK} trends shown in Fig. 10b and d).

2. Auxiliary Results

2.1. Climatological seasonal cycles from ORAS4 and Argo floats.

	sg-NPac		sg-NAtl		ml-ENA	
	Min ($Date_{min}$)	Max ($Date_{max}$)	Min ($Date_{min}$)	Max ($Date_{max}$)	(Min $Date_{min}$)	Max ($Date_{max}$)
$StrI_\sigma$ and MLD_{GP} shown in Fig. 4						
$StrI_\sigma$ ($\mathrm{kg\,m^{-3}}$)	1.34 (09 Feb)	2.33 (31 Aug)	0.11 (5 Mar)	2.85 (8 Aug)	0.14 (23 Feb)	2.43 (5 Aug)
MLD_{GP} (m)	0	107.3	0	216.8	0	181.9
Additional MLD estimations shown in Fig. S1						
MLD_{HT} (m)	0	95.7	0	162.8	0	194.4
$MLD_{\Delta\sigma}$ (m)	0	79	0	227.5	0	202.3
Alternative stratification indexes shown in Fig. 7						
G_{max} ($\mathrm{kg\,m^{-4}}$)	0.01 (17 Mar)	0.04 (20 Sep)	0.002 (21 Mar)	0.08 (8 Aug)	0.006 (9 Mar)	0.12 (8 Aug)
b_3 ($10^{-3}, \mathrm{kg\,m^{-4}}$)	4 (6 Mar)	6 (22 Jan)	0.41 (16 May)	0.84 (18 Oct)	0.27 (22 Jan)	0.76 (29 May)
Φ ($10^4, \mathrm{kg\,m^{-4}}$)	-6.7 (24 Feb)	1.4 (5 Sep)	-8.38 (28 Mar)	4.08 (16 Sep)	-4.57 (7 Mar)	0.62 (7 Oct)

Table S1. Maximum and minimum values of climatological seasonal cycles and the dates when they are reached ($Date_{min}$) and ($Date_{max}$), respectively) in 4°x4° boxes centered at the locations of the oceanographic time-series in the subtropical gyres of the North Pacific (sg-NPac) and

North Atlantic (sg-NAtl), and in the mid-latitudes of the eastern North Atlantic (ml-ENA) from ORAS4 Ocean Reanalysis data.

	sg-NPac		sg-NAtl		ml-ENA	
	Min ($Date_{min}$)	Max ($Date_{max}$)	Min ($Date_{min}$)	Max ($Date_{max}$)	(Min $Date_{min}$)	Max ($Date_{max}$)
$StrI_\sigma$ and MLD_{GP} shown in Fig. 4						
$StrI_\sigma$ ($\mathrm{kg\,m^{-3}}$)	1.15 (23 Feb)	2.11 (15 Sep)	0.39 (17 Mar)	2.87 (27 Aug)	0.03 (7 Mar)	2.17 (15 Aug)
MLD_{GP} (m)	0	131.2	0	258.9	0	2053.23
Additional MLD estimations shown in Fig. S1						
MLD_{HT} (m)	0	93.9	0	221.6	0	200.3
$MLD_{\Delta\sigma}$ (m)	0	105.89	0	259.3	0	213.4
Alternative stratification indexes shown in Fig. 7						
G_{max} ($\mathrm{kg\,m^{-4}}$)	0.01 (16 Mar)	0.04 (27 Sep)	0.005 (24 Mar)	0.1 (31 Aug)	0.003 (17 Feb)	0.11 (21 Aug)
b_3 ($10^{-3}, \mathrm{kg\,m^{-4}}$)	2 (3 Mar)	5 (18 Oct)	0.62 (1 Mar)	1 (17 Nov)	0.13 (16 Mar)	0.36 (21 Jul)
Φ ($10^4, \mathrm{kg\,m^{-4}}$)	-5.65 (05 Apr)	7.1 (18 Sep)	-8.29 (25 Apr)	3.03 (14 Sep)	-3.95 (18 Mar)	1.4 (5 Sep)

Table S2. Maximum and minimum values of climatological seasonal cycles and the dates when they are reached ($Date_{min}$) and ($Date_{max}$), respectively) in 4°x4° boxes centered at the locations of the oceanographic time-series in the subtropical gyres of the North Pacific (sg-NPac) and North Atlantic (sg-NAtl), and in the mid-latitudes of the eastern North Atlantic (ml-ENA) from Argo floats.

2.2. Seasonal cycles and long term variability from MLD_{HT} and $MLD_{\Delta\sigma}$.

In order to provide further evidence to the MLD variability obtained from the application of the Gonzalez-Pola et al. (2007) algorithm (MLD_{GP}), the climatological seasonal cycles and long

term trends obtained estimating the MLD on hydrographic profiles following the method of Holte and Talley (2009) (MLD_{HT}) and threshold method ($MLD_{\Delta\sigma}$ for $\Delta\sigma$= 0.03 kg·m^{-3}) have been analyzed, and the results are presented below.

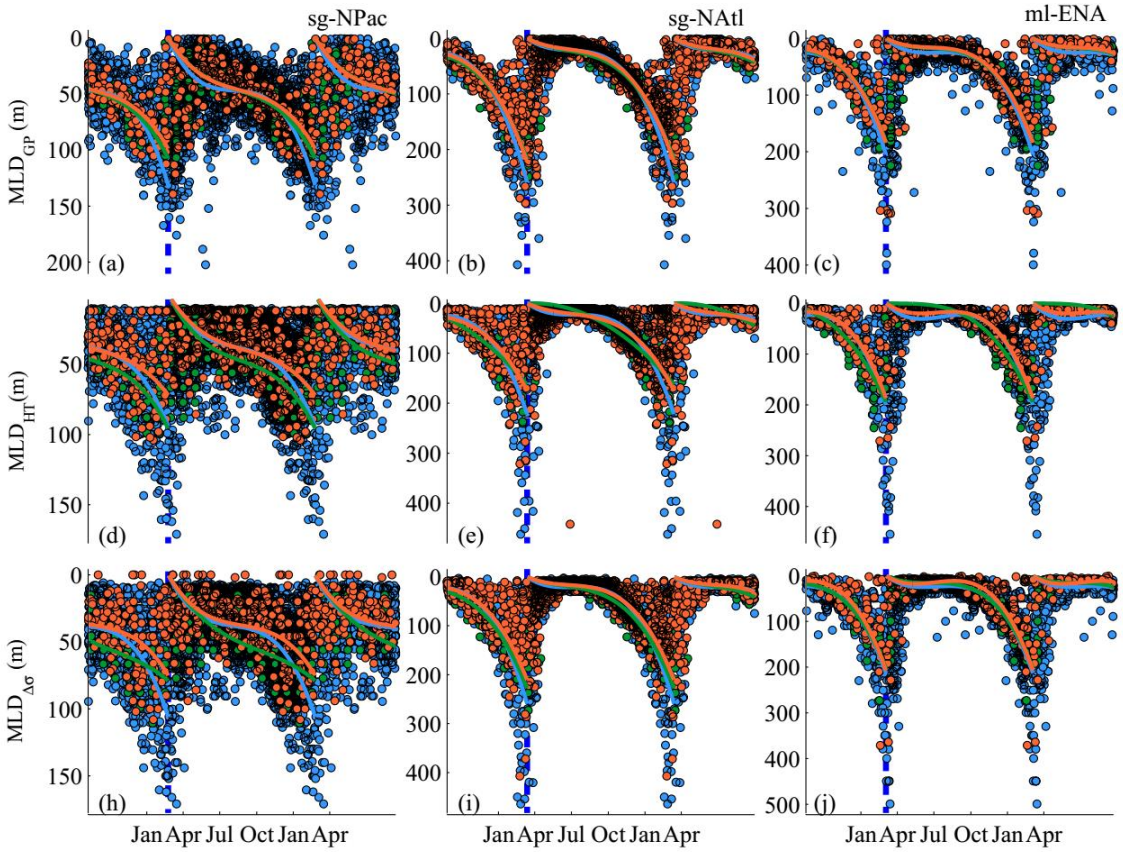

Figure S2. MLD_{GP}, MLD_{HT} and $MLD_{\Delta\sigma}$ climatological seasonal cycles. (a), (b), and (c) MLD measured as MLD_{GP} on oceanographic time-series (orange filled circles), and in 4°x4° boxes centered at the locations of oceanographic time-series from ORAS4 ocean reanalysis data (green circles), and Argo floats (blue circles). The climatological seasonal cycles using the oceanographic time-series, ORAS4 and Argo floats data are shown by the orange, green and blue lines, respectively. (d), (e), and (f) idem to (a), (b) and (c) but for MLD_{HT}. (g), (h), and (i) idem to (a), (b) and (c) but for $MLD_{\Delta\sigma}$. The vertical blue lines mark the date of minimum SST at each location.

$MLD_{\Delta\sigma}$ tends to overestimate the winter MLD when the upper ocean vertical structure consists in a deep MLD continued by a weak stratification of the permanent pycnocline. In that case, hundreds of meters in the vertical differ in very small $\Delta\sigma$, and the threshold method enlarge the MLD. This overestimation is particularly large in the ml-ENA where the deepest winter MLDs are up 150 m deeper for $MLD_{\Delta\sigma}$ than for MLD_{GP} (Fig. S1c and f). MLD_{HT} finds maximum MLDs in winter similar to MLD_{GP}. However, MLD_{HT} finds more often shallow MLDs in

comparison with MLD_{GP} and $MLD_{\Delta\sigma}$, and it makes climatological maximum winter MLD for MLD_{HT} on average 30 m shallower than for MLD_{GP}.

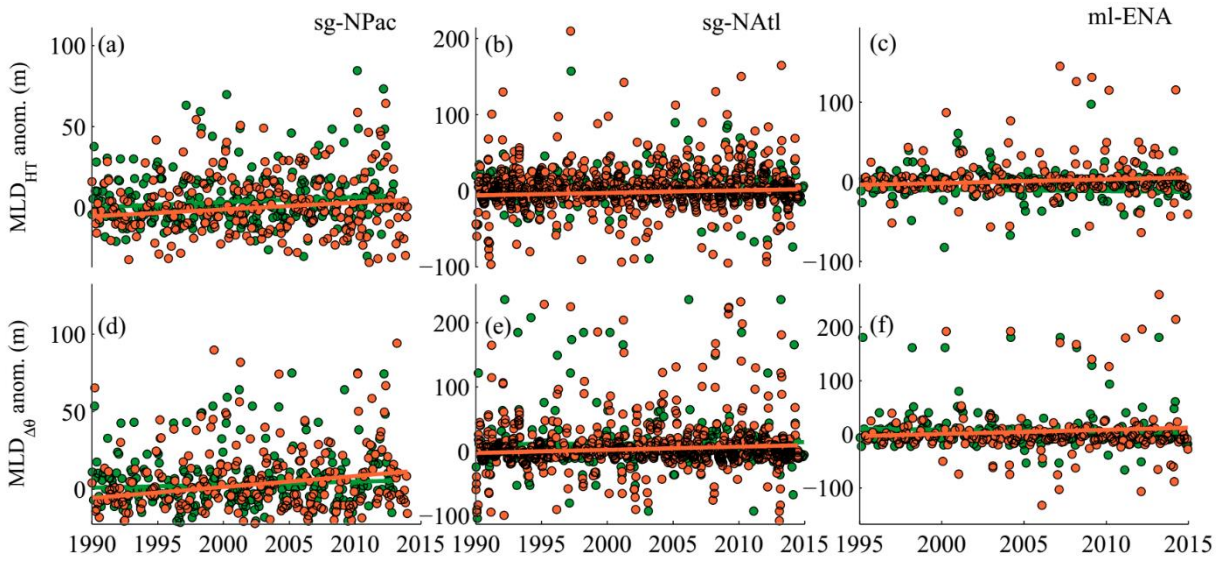

Figure S3. MLD_{HT} and $MLD_{\Delta\sigma}$ long term changes. (a), (b), and (c) anomaly time-series of MLD_{HT} estimated on oceanographic time-series (orange filled circles) and in 4°x4° boxes centered at the locations of oceanographic time-series from ORAS4 ocean reanalysis data (green circles). The linear trends using the oceanographic time-series and ORAS4 data are shown by the orange and green lines, respectively. (d), (e), and (f) idem to (a), (b) and (c) but for $MLD_{\Delta\sigma}$ anomaly time-series.